Collaborative Multi-Robot Non-Prehensile Manipulation via Flow-Matching Co-Generation

Yorai Shaoul Carnegie Mellon University yshaoul@cs.cmu.edu

> Federico Pecora Amazon Robotics fpecora@amazon.com

Zhe Chen* Amazon Robotics zhecm@amazon.com

Maxim Likhachev Carnegie Mellon University maxim@cs.cmu.com Naveed Gul Mohamed* Amazon Robotics naveedg@amazon.com

Jiaoyang Li Carnegie Mellon University jioyanl@cs.cmu.com



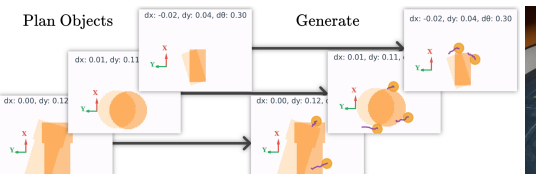






Figure 1: The Generative Collaboration (GCo) framework learns components that are hard to model and plans those that are easy: given image observations, it proposes motions for all objects, jointly generates contact points and manipulation trajectories with flow-matching co-generation, and plans multi-robot paths to convey the team to manipulation sites. From left to right: an illustration of one GCo iteration for seven robots collaboratively manipulating three large objects in a shared space.

ABSTRACT

Coordinating a team of robots to reposition multiple objects in cluttered environments requires reasoning jointly about where robots should establish contact, how to manipulate objects once contact is made, and how to navigate safely and efficiently at scale. Prior approaches typically fall into two extremes-either learning the entire task or relying on privileged information and handdesigned planners-both of which struggle to handle diverse objects in long-horizon tasks. To address these challenges, we present a unified framework for collaborative multi-robot, multi-object non-prehensile manipulation that integrates flow-matching cogeneration with anonymous multi-robot motion planning. Within this framework, a generative model co-generates contact formations and manipulation trajectories from visual observations, while a novel motion planner conveys robots at scale. Crucially, the same planner also supports coordination at the object level, assigning manipulated objects to larger target structures and thereby unifying robot- and object-level reasoning within a single algorithmic framework. Experiments in challenging simulated environments demonstrate that our approach outperforms baselines in both motion planning and manipulation tasks, highlighting the benefits of generative co-design and integrated planning for scaling collaborative manipulation to complex multi-agent, multi-object settings. Visit gco-paper.github.io for code and demonstrations.

KEYWORDS

Multi-Robot Planning, Robotic Manipulation, Generative Modeling

1 INTRODUCTION

Multi-robot collaboration is a central ambition in robotics, promising systems of robots that can accomplish tasks beyond the capabilities of an individual. A particularly compelling example is

multi-robot manipulation, where robots must physically coordinate to move and position objects in their environment. Applications range from the home, where teams of robots tidy living spaces, to warehouse logistics, where robots transport and align inventory.

Multi-robot manipulation poses unique challenges. Unlike purely navigational coordination, robots must reason about their own motions, the coupled dynamics of objects under contact, and how to assign and reassign interactions across multiple robots and objects. This coupling makes the problem complex: the space of possible robot-object assignments, contact formations, and coordinated motions grows quickly with the number of robots and objects.

Prior methods approach this challenge from two extremes. Learning-based approaches aim to capture the entire process from data, which can model complex dynamics but often sacrifices generalization and scalability [8]. Planning-based approaches [30] leverage structure to compute coordinated trajectories, but rely heavily on perfect models and can be brittle when deployed in the real world. In contrast, we argue for a middle ground: planning should be used wherever structure allows, and learning should be applied where models are uncertain or intractable to design by hand.

In this paper, we present a unified framework for collaborative manipulation that embodies this principle, with three contributions: (i) **The Generative Collaboration framework** (GCo) for scalable multi-robot, multi-object collaborative manipulation. (ii) **A flow-matching co-generation interaction model** that proposes feasible and diverse contact and motion strategies for objects observed through images alone. To the best of our knowledge, this is the first use of discrete-continuous flow-matching co-generation in robotics. And (iii) a new multi-robot motion planner (GSPI)

^{*}Equal contribution. During part of this work Yorai interned at Amazon Robotics.

 $^{^1}$ Flow-matching co-generation remains largely unexplored in robotics. The closest work [12] couples discrete task sequencing with continuous motion using hybrid diffusion. Our approach differs by directly co-generating discrete *contact points* $\mathcal K$ and continuous trajectories $\mathcal T$ within a unified flow-matching framework, enabling scalable coordination in collaborative manipulation.

that computes safe, coordinated trajectories for conveying multiple entities to goal configurations. We show that the GCo framework, and individually the GSPI algorithm, both scale more effectively than existing methods to manipulation and planning problems.

2 PROBLEM FORMULATION

We study the problem of multi-robot collaborative manipulation, where a team of robots jointly transports multiple objects to designated goal configurations through non-prehensile interactions.

Let $\mathcal{R} = \mathbb{R}^1, \mathbb{R}^2, \dots, \mathbb{R}^N$ denote the set of N robots operating in a shared workspace $\mathcal{W} \subseteq \mathbb{R}^2$. To abstract away embodiment-specific details, each robot \mathbb{R}^i is modeled as a disk of fixed radius r > 0. The configuration of robot \mathbb{R}^i is $q_R^i \in Q_R^i \subseteq \mathbb{R}^2$, and a trajectory of horizon H is defined as a sequence of timed configurations and termed τ^i , with τ^i denoting the robot configuration at time t.

The environment also contains a set of M movable *objects*, $O = \phi_1, \ldots, \phi_M$, where the configuration of object ϕ_j is given by $q_o^j \in Q_o^j \subseteq SE(2)$. The workspace may additionally contain static *obstacles* that cannot be intersected by robots or objects.

The task specifies M goal configurations $q^1_{\varphi, \mathrm{goal}}, \ldots, q^M_{\varphi, \mathrm{goal}}$. We adopt an anonymous object–goal assignment: it suffices for each goal to be occupied by some object, but not necessarily a specific one. This setting naturally models construction-style tasks, such as laying bricks to assemble a structure, where the identity of each individual brick is irrelevant.

The task objective is to compute a set of coordinated robot trajectories $\mathcal{T}=\{\tau^1,\cdots,\tau^N\}$ such that, when executed, the resulting coupled robot–object dynamics cause all objects in O to reach the set of goal configurations $\{q^i_{\sigma,\mathrm{goal}}\}_{i=1}^M$. Importantly, the trajectories need not remain fixed throughout execution. To cope with model mismatch and real-world uncertainty, our framework interleaves planning with execution, allowing dynamic replanning and reassignment of robot–object interactions as needed.

3 BACKGROUND

We now situate our work within the broader context of the robotics and AI literature. We survey related work in Sec. 3.1 and provide relevant background on flow matching for generative modeling and anonymous multi-robot motion planning in Sec. 3.2 and Sec. 3.3.

3.1 Related Work: Multi-Robot Manipulation

Much of the research on multi-robot coordination has centered on geometric collision avoidance, where robots are tasked with reaching goal positions while avoiding one another and obstacles, either in simplified 2D grid environments [16, 17, 22, 24, 27] or in realistic robotic systems [14, 15, 25, 26]. Far less attention has been given to collaboration through interaction, where robots must not only coordinate trajectories but also physically engage with objects.

Because this setting is combinatorially and physically challenging — involving assignments, motion planning, and contact dynamics — early approaches typically tackled only part of the problem or relied on strong assumptions. For instance, Hartmann et al. [11] addressed the task-and-motion planning (TAMP [9]) formulation of multi-robot rearrangement, scaling impressively with objects and robots, but disregarded robot-object physical interactions. Tang

et al. [30] considered long-horizon planning for physical manipulation, but restricted attention to a single object whose exact shape and physical parameters are known, enabling geometric analysis.

Recent work has sought to relax these assumptions by learning all aspects of collaborative manipulation directly. Feng et al. [8], along with related efforts [20, 33], pursue hierarchical reinforcement learning (HRL), in which low-level controllers handle locomotion while higher-level policies determine how robots engage with objects. Although in principle such approaches could scale, in practice they have only been demonstrated on drastically simplified problems—typically no more than two or three robots, a single object, and environments with few or no obstacles. Even within these restricted settings, HRL policies often struggle with large transformations and obstacle avoidance. By contrast, our work introduces algorithms designed to scale explicitly with both the number of robots and the number of objects, even in cluttered spaces where robots may be outnumbered by objects or vice versa.

Considering existing methods that either plan under strong modeling assumptions or learn from scratch in restricted settings, an opportunity exists for approaches that leverage structure where possible and reserve learning for what is hard to model. Our perspective is that collision-free navigation, task assignment, and motion planning are structured subproblems that benefit from planning, while the generation of contact strategies — determining how robots should engage with objects and coordinate their influence — is best learned from data. This view is supported by recent advances in diffusion and flow-matching models for imitation learning, which show that demonstrations can efficiently convey local coordinated behaviors [1, 3, 5], and by the success of multi-agent path finding (MAPF) algorithms [23, 24], which can reliably assign and convey large robot teams between locations in simplified environments.

3.2 Background: Flow-Matching Co-Generation

Flow-matching, a flexible method for generative modeling, has recently found success in various domains, including imitation learning for robotics [1], image generation [18], and protein design [2]. In this work, we leverage flow-matching models to determine the number of contact points to create with objects, where to place them, and how to move once contact is established. Let us begin with background on three flavors of flow-matching: continuous, discrete, and continuous-discrete co-generation.

Continuous Flow Matching casts generation as learning a time-dependent velocity field u_t that transports a base distribution p_0 into the data distribution p_1 [18]. For an interpolated sample

$${}^{t}X := ({}^{1}X - {}^{0}X)t + {}^{0}X$$

between a noisy sample ${}^{0}\!X \sim p_{0}$ and a data sample ${}^{1}\!X \sim p_{1}$, the flow matching objective is to learn an estimated velocity field u_{t}^{θ} that matches the sample velocity with its estimated velocity.

$$\theta^* = \arg\min_{\theta} \mathbb{E}_{0X \sim p_0, {}^1\!X \sim p_1, t \in [0,1]} \|({}^1\!X - {}^0\!X) - u^{\theta}_t({}^t\!X)\|^2.$$

Generating new samples ${}^{1}\hat{X}$ is done by integrating the ODE

$$\frac{d}{dt}{}^{t}X = u_{t}^{\theta}({}^{t}X), \quad {}^{0}X \sim p_{0}, \quad {}^{1}X = {}^{0}X + \int_{0}^{1} u_{t}^{\theta}({}^{t}X)dt. \tag{1}$$

While flow-matching is powerful for continuous data (e.g., trajectory waypoints), categorical domains where samples are sequences

of values from a fixed set (e.g., choosing contact points from a finite set of image pixels) benefit from a different treatment.

Discrete Flow Matching [10] is a framework for generating sequences K of discrete samples when elementes can only take on values from a discrete, finite, state space \mathcal{K} . Let a sample from the space of discrete sequences of length $B \in \mathbb{Z}^{>0}$ elements be

$$K := \{K^{(1)}, K^{(2)}, \cdots K^{(B)} \mid K^{(b)} \in \mathcal{K}\}.$$

Given an initial "noisy" discrete sequence ${}^{0}\!K \sim p_{\rm d,0}$ and a data sequence ${}^{1}\!K \sim p_{\rm d,1}$, an interpolated sample is obtained by mixing

$${}^{t}K^{(b)} \sim \operatorname{Cat}((1-t)\delta_{0K^{(b)}} + t\delta_{1K^{(b)}}),$$

where δ is the Dirac delta function and Cat is the categorical distribution. Simply put, value $K^{(b)} \in {}^t\!K$ takes on the base value ${}^0\!K^{(b)}$ with probability (1-t) or the data value ${}^1\!K^{(b)}$ with probability t.

The discrete flow matching objective is to predict $\delta_{^1\!K}$ directly from an interpolated $^t\!K$. This prediction, which is sampled from the generated distribution $u_{\mathrm{d},t}^\phi(^t\!K)$ named the discrete velocity, is supervised with a cross-entropy (CE) loss

$$\phi^* = \arg\min_{\phi} \ \mathbb{E}_{0K \sim p_{\mathbf{d},0}, \ ^1\! K \sim p_{\mathbf{d},1}, \ t \in [0,1]} \left[\sum_{b=1}^B \mathrm{CE} \left(u_{\mathbf{d},t}^{\phi}(^t\! K^{(b)}), \ \delta_{^1\! K^{(b)}} \right) \right].$$

Generating new discrete samples ${}^{1}\!\hat{K}$ is done by simulating a categorical Markov chain, where each element $K^{(b)}$ transitions according to the predicted discrete velocity $u_{\mathrm{d}\,t}^{\phi}$ over $t\in[0,1]$,

$${}^{0}K \sim p_{\mathrm{d},0}, \quad {}^{t+\Delta t}K^{(b)} \sim \mathrm{Cat}\left(u_{\mathrm{d},t}^{\phi}({}^{t}K^{(b)})\right)$$
 (2)

The base distribution $p_{d,0}$ we adopt in this work is the "mask" distribution where all elements are set to a single value [M].

Flow-Matching Co-Generation [2] attempts to jointly generate tightly coupled discrete and continuous samples. Let a joint state be $({}^t\!K,{}^t\!X)$ where ${}^t\!K$ denotes discrete valued sequence and ${}^t\!X$ denotes continuous valued samples. A co-generative flow-matching model learns a pair of velocity fields

$$u_{\mathrm{d},t}^{\phi}({}^{t}X,{}^{t}K), \quad u_{\mathrm{c},t}^{\theta}({}^{t}X,{}^{t}K),$$

where $u_{\mathrm{c},t}^{\theta}$ is a continuous velocity and $u_{\mathrm{d},t}^{\phi}$ is a discrete velocity, both conditioned on the discrete and continuous variables (Fig. 7). The training objective is the sum of continuous and discrete flow-matching losses, and generating new joint samples (${}^{1}\!\hat{K}, {}^{1}\!\hat{X}$) is done by simultaneously integrating the continuous ODE (Eq. 1) and evolving the discrete state ${}^{t}\!K$ via a categorical Markov chain with transition probabilities given by $u_{\mathrm{d},t}^{\phi}({}^{t}\!X, {}^{t}\!K)$ (Eq. 2), both starting from (${}^{0}\!X, {}^{0}\!K$) $\sim (p_{0}, \delta_{\mathrm{[M]}})$. In this work, we show that flow-matching co-generation can be an effective choice for learning contact points and manipulation trajectories.

3.3 Background: AMRMP

Anonymous multi-robot motion planning (AMRMP) is a foundational problem in robotics: given N robots with start configurations $Q_{R,\text{start}} \in Q_R^1 \times Q_R^2 \times \cdots \times Q_R^N$ and a set of interchangeable goals $Q_{R,\text{goal}}$, the task is to compute safe trajectories \mathcal{T} such that the collection of terminal states coincides with $Q_{R,\text{goal}}$.

Most prior work on AMRMP has studied the graph-based abstraction known as anonymous multi-agent path finding (AMAPF), where robots are modeled as points moving along vertices and edges [13, 23, 28, 29, 34]. Within this setting, many methods focus on optimal or bounded sub-optimal path finding and goal assignments, often building on Conflict-Based Search (CBS) [27] to leverage its strong theoretical guarantees. Other approaches emphasize scalability over optimality. TSWAP [23], for instance, is a highly efficient rule-based algorithm that detects potential deadlocks and resolves them by swapping goals between robots.

Encouraged by the success of algorithms in these discrete point-robot domains, recent works have extended MAPF—the non anonymous counterpart to AMAPF—to continuous settings by replacing grid edges with *motion primitives*, short kinematically feasible transitions between configurations [6, 25, 26]. Adapting CBS-like methods to use motion primitives preserves their theoretical guarantees, but much of their efficiency is lost without grid-specific enhancements, raising doubts about the practicality of CBS-based AMAPF algorithms in this setting. It is therefore natural to consider applying motion primitives to highly efficient rule-based methods like TSWAP. Unfortunately, TSWAP's goal-swapping rule assumes that an exchange always resolves a deadlock, an assumption that fails for robots with volume, leading to repeated unproductive swaps.

In this work, we introduce GSPI ("Giuseppe"), a new AMRMP algorithm that combines the efficiency of rule-based MAPF methods with the deadlock resolution strategies inspired by TSWAP and DEC-UNAV [7], adapted to motion-primitive domains without introducing deadlocks or livelocks. GSPI forms a central building block of our generative collaboration framework, and with this background in place we now turn to its introduction.

Algorithm 1 GCo: Generative Collaboration for Multi-Robot Manipulation

4 GENERATIVE COLLABORATION

Despite substantial advances in multi-robot planning and learning, existing approaches fall short of addressing collaboration at scale in a physically grounded way. To this end, we introduce GCo—a framework for interleaving learning and planning in collaborative multi-robot systems. The core principle of GCo is simple:

plan what can be modeled well, and learn what cannot.

In the context of non-prehensile manipulation, we identify two distinct operation modes that must be addressed by a team of robots: they must generate manipulation motions that define how robots interact with objects to induce desired transformations, and they must generate cooperative motions that bring robots into the appropriate configurations to realize those interactions. Manipulation motions depend on objects' physical dynamics as well as stochasticity in execution—making them natural candidates for learning. In

contrast, cooperative motions involve the geometric feasibility of moving multiple entities through clutter, a domain where planning excels. GCo unifies these two modes in a closed-loop framework, interleaving generation of data-driven manipulation motions and planning of cooperative trajectories to realize them (Alg. 1).

Each iteration begins with perception (line 2). Objects ϕ_i are observed via images \mathcal{I}^j , which are $w \times w$ occupancy matrices, and the current world state X_w is updated with the states of robots and obstacles. Next, the planner GSPI is invoked at the object-level to generate short-horizon trajectories $\tau_{\rm obj}^j$ for each object (line 3), from which short transformation subgoals T^{j} are extracted (line 4). Robots are then budgeted² across all objects with non-zero T^{j} , each receiving B^{j} robots (line 5). Finally, the learned manipulation policy, termed π_{θ} , co-generates object-centric contact points \mathcal{K}^{j} and manipulation trajectories $\mathcal{T}_{\mathrm{manip}}^{j}$ conditioned on images, transforms, and robot budgets (line 6). To realize these motions, GSPI is called a second time at the robot level to compute cooperative trajectories \mathcal{T}_{coop} , which bring robots to contact points (line 7). Once computed, these free-space cooperative trajectories are concatenated with the corresponding manipulation trajectories that begin at the reached contact points and are then executed (line 8). This process advances the system toward the object-goal set, and the loop repeats until all object-goals have been achieved.

In the following sections, we detail GCo's manipulation module (Sec. 4.1), describe the GSPI algorithm (Sec. 4.2), and present experiments (Sec. 5) comparing GCo and GSPI to existing baselines.

4.1 Learning Non-Prehensile Manipulation with Flow-Matching Co-Generation

Our objective is to endow teams of robots with the ability to generate object-level manipulation motions that achieve target transformations $T^j \in SE(2)$. Central to this problem is deciding both where robots should make contact with objects and how they should move once contact is established. We pursue a flow-matching approach and introduce three instantiations: GCo_{CT} , which treats the task as a monolithic synthesis problem by directly generating continuous trajectories without explicit contact modeling; GCo_{CC}, which co-generates contact points and trajectories jointly in continuous space, parameterizing contacts in the object frame and trajectories as short waypoint sequences; and GCoDC, which anchors contact points in the perceptual space through discrete selection while generating trajectories continuously. All three methods are effective and consistently outperform baselines, while the co-generation variants provide added stability, with the discrete-continuous formulation proving the most reliable in challenging tasks (Sec. 5).

4.1.1 **Direct Continuous Trajectory Generation (GCo**_{CT}). In GCo_{CT}, multi-robot manipulation is posed as generating only robot trajectories and treating their first state as a contact point:

$$\mathcal{T}_{\text{manip}}^{j} \in \mathbb{R}^{B_{\text{max}} \times H \times 2}$$

I.e., $\mathcal{T}_{\mathrm{manip}}^{j}$ is a container for B_{max} trajectories (a maximum budget), each of length H, whose values are unconstrained. Executing $\mathcal{T}_{\mathrm{manip}}^{j}$

should transform o_j by T^j . To generate, a flow-matching model evolves noise ${}^0\mathcal{T}^j_{\mathrm{manip}} \sim \mathcal{N}(\mathbf{0}, \mathbf{I})$ into structured trajectories via integration of a learned conditional velocity field u^θ_t :

$$\mathcal{T}_{\mathrm{manip}}^{j} = \int_{0}^{1} u_{t}^{\theta}({}^{t}\mathcal{T}_{\mathrm{manip}}^{j} \mid \mathcal{I}^{j}, T^{j}, B^{j}) dt.$$

While conceptually simple, this approach requires reasoning about a high-dimensional space; generating unconstrained sequences of waypoints across all robots can be difficult to learn.

4.1.2 **Continuous–Continuous Co-Generation (GCo** $_{CC}$). To simplify the learning problem, GCo $_{CC}$ decomposes generation into two structured continuous components:

$$\mathcal{K}^j = \{k^{j,b} \in \mathbb{R}^2\}_{b=1}^{B_{\max}}, \qquad \mathcal{T}^j_{\text{manip}} = \{\tau^{j,b} \in \mathbb{R}^{H \times 2}\}_{b=1}^{B_{\max}},$$

where \mathcal{K}^j are contact points in the local object frame and $\mathcal{T}^j_{\text{manip}}$ are manipulation trajectories rooted at the origin. For execution, trajectories $\tau^{j,b}$ are translated to begin at their contact point $k^{j,b}$.

A flow-matching model learns two velocity fields, u_t^{θ} and u_t^{ϕ} for contacts and trajectories, and jointly evolves $(\mathcal{K}^j, \mathcal{T}_{\mathrm{manip}}^j)$ from noisy seeds $({}^0\mathcal{K}^j, {}^0\mathcal{T}_{\mathrm{manip}}^j)$. In practice, we couple Euler integration for both continuous components to obtain ${}^1\mathcal{K}^j, {}^1\mathcal{T}_{\mathrm{manip}}^j$:

$$\begin{split} ^{t+\Delta t}\mathcal{K}^j &= \, ^t\!\mathcal{K}^j + u_t^\theta(^t\!\mathcal{K}^j,^t\!\mathcal{T}_{\mathrm{manip}}^j \mid I^j,T^j,B^j)\Delta t \\ ^{t+\Delta t}\mathcal{T}_{\mathrm{manip}}^j &= \, ^t\!\mathcal{T}_{\mathrm{manip}}^j + u_t^\phi(^t\!\mathcal{K}^j,^t\!\mathcal{T}_{\mathrm{manip}}^j \mid I^j,T^j,B^j)\Delta t. \end{split}$$

This decomposition reduces complexity by explicitly modeling structure—where to create contact, and how to move—but still requires continuous contact generation, which unnecessarily reasons over a space larger than the perceptual input space.

4.1.3 **Discrete–Continuous Co-Generation (GCo**_{DC}). Our key contribution is the discrete–continuous formulation GCo_{DC} , which couples the two components in different representational spaces. We introduce discrete contact point generation, where contacts are selected directly from the finite set of pixels in the observed image. We write a state \mathcal{K}^j , holding information about B_{\max} contact points for an object ϕ_j , as a sequence of $2B_{\max}$ discrete tokens $\{c_j^i\}_{j=1}^{2B_{\max}}$, with each consecutive pair being equivalent to an (x,y) pixel coordinate in the image frame. Formally:

$$\mathcal{K}^j := \bigg\{\underbrace{c_1^j, c_2^j}_{k_i^j}, \cdots, \underbrace{c_{2B_{\max}-1}^j, c_{2B_{\max}}^j}_{k^{j,B_{\max}}} \ \bigg| \ c_i^j \in \mathcal{K} = \{1, \dots, w\} \cup \{\texttt{[M]}\}\bigg\}.$$

Notationally, we write $(\mathcal{K}^j)^{(i)}$ to denote the i^{th} token in the state. This formulation anchors the contact point space to perceptual evidence while the set of manipulation motions remains flexible in $\mathbb{R}^{B_{\max} \times H \times 2}$. Like before, each trajectory is rooted at the origin and later shifted to its generated contact point.

To generate new contact points and manipulation trajectories \mathcal{K}^j , $\mathcal{T}^j_{\mathrm{manip}}$, we couple Euler integration for the continuous component with Markov chain transitions for the discrete component:

$$\begin{split} &(^{t+\Delta t}\mathcal{K}^{j})^{(i)} \sim \mathrm{Cat}\left(\left(u_{\mathrm{d},t}^{\theta}(^{t}\mathcal{K}^{j},^{t}\mathcal{T}_{\mathrm{manip}}^{j} \mid I^{j},T^{j},B^{j}\right)^{(i)}\right) \\ &^{t+\Delta t}\mathcal{T}_{\mathrm{manip}}^{j} = {}^{t}\mathcal{T}_{\mathrm{manip}}^{j} + u_{\mathrm{c},t}^{\phi}(^{t}\mathcal{K}^{j},^{t}\mathcal{T}_{\mathrm{manip}}^{j} \mid I^{j},T^{j},B^{j})\Delta t. \end{split}$$

4.1.4 **Variable Robot Budget**. In practice, only a limited number of robots may be available for manipulation. Training separate

²Many resource allocation schemes are possible for assigning robots to objects. In this work, we employ a simple paradigm. We allocate robots as evenly as possible across all objects that need to be manipulated, with idle robots sent to wait at safe locations. In cases with more objects than robots, robot-object pairs are matched by proximity.

models for each team size would be inefficient, so instead we train a single model that respects a robot budget B. This is achieved by creating a model that always produces B_{\max} contacts and manipulation trajectories, and training it to mask entries that are not needed. Specifically, we use the special token <code>[M]</code> to denote unused robots: in the discrete case, $k^{j,b} = (\texttt{[M]}, \texttt{[M]})$; in the continuous case, contacts within ε of the mask token's value are treated as masked, i.e., when $\|k^{j,b} - (\texttt{[M]}, \texttt{[M]})\| < \varepsilon$. In training, supervision penalizes generated budgets \hat{B}^j exceeding the allocated budget B^j : $\mathcal{L}_{\text{budget}} = \sum_{j=1}^{M} \text{ReLU}(\hat{B}^j - B^j)$.

Algorithm 2 GSPI: Goal Swapping with Priority Iritance Blue lines are modifications to the PIBT algorithm.

```
Require: Robot set \mathcal{R} = \{R^1, \dots, R^N\} with configurations q_R^i \in \mathcal{Q}_R^i, anonymous
               goals Q_{R,\mathrm{goal}}, motion-primitive generators \mathcal{G}^i(q_R^i), initial priority order
                \prec, current target map g: \mathcal{R} \rightarrow Q_{R,\mathrm{goal}}
  1 Initialize \prec to \prec_{init}, random non-repeating, numbers in [0, 1].
  2 while some R^i not at any goal do
                                                                                ▶ Edge reservations (per step).
  4
           for each R^i in \prec do TrySwap(R^i, g)
           for each R^i in \prec do TryMove(R^i)
  5
           Commit \mathcal{E}; update q_R^i; demote robots now on goals to \prec_{\text{init}}, increment others
  7 return \mathcal{T}
  8 function TryMove(R^i)
           \mathcal{E}^i \leftarrow \mathcal{G}^i(q_R^i); order by heuristic to g(R^i)
           for each e^i \in \mathcal{E}^i do
 10
                                                       ▶ Choose candidate primitives (named edges).
                 if \exists e^j \in \mathcal{E} with edge–edge conflict, continue \triangleright Higher-priority conflict.
 11
                 U \leftarrow \{R^j \neq R^i \mid R^j \text{ unreserved in } \mathcal{E}\}
 12
                                                                                  ▶ Unassigned, lower-priority.
                 S \leftarrow \{R^j \in U \mid e^i \text{ edge-state conflicts } q_R^j\}
                                                                                                 ▶ "Stepped-on" set.
 13
                if S = \emptyset then \mathcal{E} \leftarrow \mathcal{E} \cup \{e^i\}; return true
 14
                 \mathcal{E}_{curr} \leftarrow \mathcal{E}
 15
                                                                        ▶ Record current edge reservations.
                 \mathcal{E} \leftarrow \mathcal{E} \cup \{e^i\}
                                                                                ▶ Tentatively commit to edge.
 16
                 for each permutation \pi of \mathcal S do
 17
                      ok \leftarrow true
for each R^j \in \pi do
 18
                           if not TRYMOVE(R^j) then ok \leftarrow false; break
 20
 21
                       if ok then return true
                                                                              ▶ All recursive calls succeeded.
                      else \mathcal{E} \leftarrow \mathcal{E}_{curr}
                                                                                                            ▶ Roll back.
           \overline{e_{\text{wait}}^i} \leftarrow (q_R^i \rightarrow q_R^i); \quad \mathcal{E} \leftarrow \mathcal{E} \cup \{e_{\text{wait}}^i\}; \quad \text{return false}
 23
 24 function TrySwap(R^i, g)
           for each R^j with R^{\tilde{i}} \prec R^j do
 25
                                                                       ▶ Consider all lower priority robots.
 26
                d_{i,a}, d_{i,b} \leftarrow \operatorname{dist}(q_R^i, g(R^i)), \operatorname{dist}(q_R^i, g(R^j))
 27
                 d_{j,a}, d_{j,b} \leftarrow \operatorname{dist}(q_R^j, g(R^j)), \operatorname{dist}(q_R^j, g(R^i))
                if d_{i,b} < d_{i,a}
                                                                    {} \triangleright \stackrel{\cdot \cdot}{\mathbf{S}} \mathbf{wap} benefits higher-priority robot.
 28
                    and d_{i,b} + d_{j,b} \le d_{i,a} + d_{j,a} then
                                                                              ▶ Swap does not harm system.
                      \operatorname{swap} g(R^i) \leftrightarrow g(R^j)
                      swap \prec (R^i) \leftrightarrow \prec (R^j)
```

4.2 GSPI: Robot- and Object-Level Anonymous Multi-Robot Motion Planning

Once manipulation strategies are generated by π_{θ} (Sec. 4.1), robots must be routed to contact points without collisions or deadlocks. This stage falls under AMRMP: robots move in continuous space, are indistinguishable, and must reach a set of interchangeable goals. We therefore need an algorithm capable of efficiently routing large robot teams to their designated contact points—even when operating in extremely tight proximity to obstacles. Existing AMRMP planners such as C-UNAV handle open spaces effectively but struggle when robots must approach object surfaces or navigate narrow clearances (Sec. 3)—a key requirement in our setting.

One might instead extend scalable AMAPF algorithms from point-robot grids to continuous motion-primitive domains, but naïve adaptations either impose coarse discretizations or introduce deadlocks (Sec. 3.3). To address these challenges, we combine the efficiency of grid-based methods such as PIBT and TSWAP with the deadlock-avoidance logic of C-UNAV to develop GSPI, a new AM-RMP algorithm that preserves scalability while remaining robust in continuous, cluttered environments. Specifically, GSPI generalizes PIBT—a non-anonymous algorithm originally designed for point robots on regular grids—to the anonymous setting with circular robots and motion primitives. The remainder of this section details the design of GSPI, starting from PIBT and outlining how our extensions overcome its limitations.

4.2.1 Priority Inheritance with Backtracking (PIBT). PIBT [24] is a decentralized multi-agent path-finding algorithm for point robots traversing edges and vertices on a shared graph. Shown in Alg. 2 in black, PIBT assigns each robot a dynamically changing priority (line 1) and operates in discrete timesteps. At each step, PIBT iterates through robots by priority and asks each to commit to an action (TryMove in line 5).

On a robot's turn, it first sorts its available actions (transitions along edges incident to its current vertex) by a heuristic-typically how much progress each action makes toward its goal (line 9)-and prunes out any actions that collide with obstacles or higher-priority robots. From the remaining valid transitions, if its best option does not collide with any other robot's position, it commits to that action (line 14). Otherwise, it identifies the blocking robot and requests it to move away (line 20). This is implemented by calling TRYMOVE on the blocking robot, temporarily granting it the higher robot's priority so it can push away any lower-priority robots that obstruct it. This recursive chain continues until all robots commit to collisionfree actions, accommodating the request of the initiating robot. If a recursive call fails-meaning a robot cannot find a feasible move-the algorithm backtracks and tries the next-best action for the parent robot. If all options fail, the robot waits (line 23). Finally, the motions are executed, completing one timestep (line 6).

4.2.2 Limitations of PIBT. An important detail in PIBT is that priorities of robots en route to their goals gradually increase, while those of robots that reach their goals are reset to the lowest level (line 6). This rule ensures that active robots take precedence over stationary ones and contributes to PIBT's remarkably efficient planning in structured environments. However, this procedure can also create livelocks: when goals and paths overlap, a robot that has just reached its goal loses priority and may be pushed away by another. Once the displacing robot reaches its own goal, its priority drops in turn, allowing the first robot to push back. The two can continue alternating endlessly. This failure mode stems from PIBT's strict assumption of fixed goal assignments.

In our manipulation framework, this assumption is overly restrictive. Given contacts generated by π_{θ} , any robot can occupy any contact. Capitalizing on this flexibility, we develop Goal Swapping with Priority Inheritance (GSPI): an AMRMP planner for non-point robots with motion primitives that shares PIBT's efficiency and lightweight structure while also eliminating livelocks by introducing a goal swapping mechanism.

4.2.3 **The GSPI Algorithm**. At its core, GSPI follows the structure of PIBT and operates in iterations, where in each iteration robots commit to actions and execute them. In PIBT, each iteration consists solely of a *move* stage (line 5), where robots select and execute

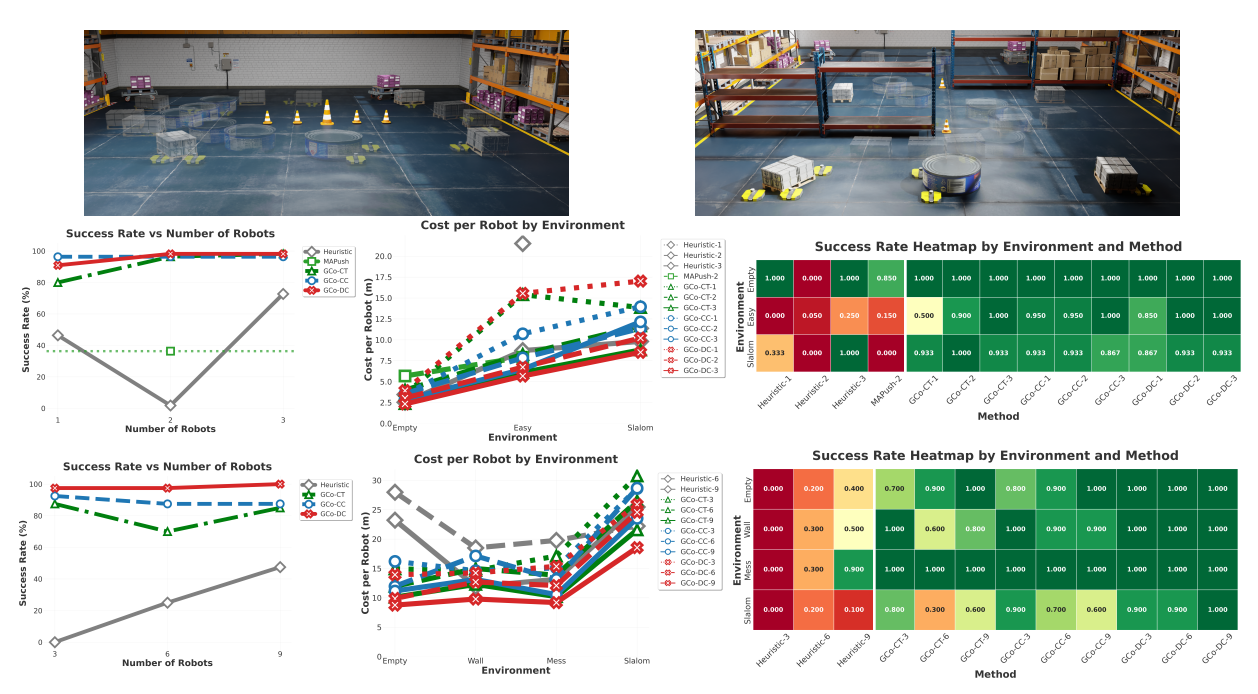


Figure 2: Performance and scalability analyses for multi-robot multi-object manipulation. Middle and bottom rows: results for single- and multi-object manipulation, respectively. We report overall success rates (left column), overall average distance traveled per robot (middle), and a breakdown of success rates. Numbers following method names denote the number of robots available in the scene. GCo methods consistently outperformed MAPUSH and HEURISTIC baselines with GCo_{DC} performing the best. Top: Wall and Slalom setups. Find additional visualizations in Appendix A.1.

actions. In GSPI, we add the *swap* stage (line 4), where robots may exchange goals with each other.

The *move stage* resembles that of PIBT but includes modifications that extend it to continuous domains with disk-shaped robots. In PIBT, where robots are modeled as points, each candidate action corresponds to traversing a graph edge and can, at most, be blocked by a single other robot located at the destination vertex. In contrast, GSPI operates with motion primitives and non-zero robot footprints. As a result, a candidate action may intersect several lower-priority robots if their configurations overlap with the swept area of the primitive. To handle this, GSPI constructs the set $\mathcal S$ of all affected robots (line 13) and asks them to yield to the higher-priority robot by creating a recursive TRYMOVE call for each one, with later recursive calls treating earlier ones as higher-priority (line 20). GSPI explores all orderings of affected robots in $\mathcal S$ (line 17); if one ordering succeeds, the motion is accepted, and otherwise, the system rolls back (line 22) and tries the next candidate primitive.

In the *swap stage*, GSPI iterates over robots by priority and evaluates whether exchanging goals and priorities between pairs would improve overall progress. A swap is proposed for a pair when two conditions hold (line 28): (i) the higher-priority robot is closer to the other's goal than to its own, and (ii) the exchange does not increase the total team distance. If both are satisfied, the robots swap goals and priorities (lines 29 and 30). The goal-swapping stage serves two key purposes. First, it relaxes fixed robot—goal assignments and promotes efficient routing in the *anonymous* case, where any robot may occupy any goal. Second, it eliminates the livelocks that arise in PIBT's fixed-goal formulation, where robots can repeatedly push one another without either remaining at a goal. Intuitively, livelocks

occur in PIBT when a high-priority robot pushes a lower-priority robot off its goal and continues to push until reaching its own goal. In GSPI, such a situation triggers a goal swap: the higher-priority robot simply takes the closer goal, removing the need for the two robots to move head-to-head, and avoids a livelock.

Empirically, these mechanisms yield a fast and scalable AMRMP algorithm (Sec. 5.3), and theoretically, GSPI is *complete* under some assumptions (Appendix B). In this work, we use GSPI both to convey robots to their assigned contact points, where we run it until all robots occupy goals (Alg. 1, line 7), and to compute transformations T^j for each object ϕ_j by invoking GSPI at the object level for two iterations (Alg. 1, lines 4 and 3).

5 EXPERIMENTAL EVALUATION

We evaluated GCo across diverse scenarios to assess its ability to generate coordinated manipulation strategies and scalable multirobot motion plans. In our experiments we sought to address three questions: (i) How well does GCo handle single-object manipulation compared to HRL and heuristic baselines? (ii) How does GCo scale to tasks with more robots and objects? (iii) Can GSPI scale to large-scale AMRMP problems? To this end, we constructed three suites of problems covering challenging manipulation and planning settings. In 286 manipulation tasks with up to 5 objects and 9 robots, we varied object shape, size, and the number of available robots. In another 270 motion-planning tasks with up to 125 robots, we varied obstacle complexity and robot count. Compiled results are in Fig. 2 and 3, with additional illustrations and results in Appendix A.1.

We focused on two primary metrics: success rate and solution cost. In manipulation tasks, success was declared when all objects

reached their target configurations within 0.15 meters in translation and 0.5 radians in orientation. Solution cost was measured as the average distance traveled per robot to execute motions. In motion-planning tasks, success was declared when collision-free trajectories for all robots from their starts to goals were found. Solution cost was the sum of distances traveled by robots.

5.1 Single-Object Manipulation

We began with simple single-object manipulation problems (Fig. 2 middle row), where small teams were tasked with collaboratively moving and reorienting a square object to a target configuration.

5.1.1 Evaluated Methods. To disentangle the contribution of different design choices, we included all three variants of GCo. The trajectory-only model (GCo $_{CT}$) generated unconstrained trajectories, with the first configuration serving as a contact point. The continuous–continuous co-generation model (GCo $_{CC}$) predicted both contact points and trajectories in continuous space. Finally, the discrete–continuous co-generation method (GCo $_{DC}$) integrated discrete contact-point selection with continuous trajectory generation. All models were trained on the same data: 20,000 samples of variable-sized boxes and cylinders for 1000 epochs. Data was collected by rolling out motions of different team sizes and contact formations within MuJoCo [31] and recording the outcomes.

We compared our approaches against two baselines. The first was MAPush [8], a recent reinforcement-learning method for multiagent pushing using quadrupedal robots. We used its official implementation³, trained models, and supplied object shapes. Since only two-robot models were provided, we report results for this team size only (Fig. 2). For our second baseline, we developed a heuristic method inspired by Chen et al. [4]. This baseline, HEURIS-TIC, operated similarly to GCo, but replaced GCo's contact-point and trajectory generation policy π_{θ} with a heuristically defined procedure. Given an object o_i and requested transformation T^j , HEURISTIC chose contact points for the object by placing one to three contact points (depending on the allocated budget) five centimeters behind the object observation's center, aligned perpendicular to the requested displacement vector. Then, it computed manipulation trajectories by transforming the contact points with T^{j} and linearly interpolating between the chosen and transformed contact points. If contacts overlapped with the object, the points (and consequently the trajectories too) were radially shifted away from the object observation centroid.

5.1.2 **Test Problems**. This first suite of tasks considered a single square object and robot team sizes varying from one to three. We evaluated in three environments. In the *Empty* setting and the *Easy* setting, the object was tasked to move one meter without rotation or two meters and be rotated by 2 radians, respectively. In both, we tested motions in $\pm x$ and $\pm y$ directions, with the *Empty* setting being obstacle-free and the *Easy* setting having an obstacle between start and goal. In the *Slalom* setting, the object was tasked to be maneuvered from the bottom to the top of a maze-like environment, requiring long-horizon coordination (illustrated in Appendix A.1).

To accommodate its original design, the problems given to MA-Push were easier than those posed to GCo and Heuristic. Specifically, MAPush used a looser termination condition with a tolerance of 0.5 meters (instead of 0.15), and ignored orientation completely. GCo and Heuristic were capped at 100 manipulation actions to complete tasks, and MAPush was allocated 2 simulation minutes. Both limits were intentionally generous, as our focus was on assessing each method's ability to complete the manipulation tasks successfully rather than on how quickly it could do so; the time limits merely served to end runs that entered irrecoverable states or made progress at a negligible rate.

5.1.3 **Results**. Our results (Fig. 2 middle) show that all three GCo variants consistently achieved higher success rates and lower costs than the baselines. MAPUSH performed well in simple cases but failed in tasks requiring longer horizons, often struggling even in the Easy environment. The heuristic baseline exhibited inconsistent performance, solving Empty tasks with one and three robots but failing with two. One failure mode was due to contacting the object from its sides, slipping rather than pushing effectively. With three robots, however, it solved most simple problems well. By contrast, GCo solved nearly all problems with low costs. We observed that solution costs per robot decreased as team size increased, suggesting that GCo efficiently uses available resources (Fig. 6).

5.2 Multi-Object Manipulation

We next considered significantly more complex scenarios where multiple objects were required to be simultaneously manipulated to goals with more extreme displacements and orientations. Find illustrations in the top row of Fig. 2, and results at the bottom row.

- 5.2.1 **Evaluated Methods**. We evaluated the same three GCo variants and the Heuristic baseline, and excluded MAPush as it was not designed to manipulate multiple objects simultaneously.
- 5.2.2 **Test Problems**. Teams of three, six, or nine robots were asked to manipulate up to five objects over translations of up to six meters and rotations of roughly 2.5 radians, which is far more demanding than settings considered in prior work [8].

We reused *Empty* and *Slalom* from the single-object tasks, only this time with more objects, and added two new settings: *Wall* and *Mess*. In the *Empty* environment, five objects were required to move between two rows of goals. We initially assigned object starts and goals diagonally across the rows, making the initial object–goal assignment maximally difficult and requiring goal swaps for efficient solutions. In the *Wall* environment, a wide obstacle blocked the center, and goal assignments for three randomly varying objects were deliberately convoluted. In the *Slalom* environment, five objects were asked to traverse tight corridors in a maze, where poor coordination can easily cause deadlocks or collisions that block progress. The new *Mess* setting included four objects in an empty space required to be arranged in a square formation.

5.2.3 **Results**. The results (Fig. 2 bottom row) highlight the challenges of multi-object manipulation. The heuristic baseline failed entirely with three robots and struggled with larger teams, mainly due to its inability to handle rotations effectively. Among the GCo

 $^{^3} https://github.com/collaborative-mapush/MAPush\\$

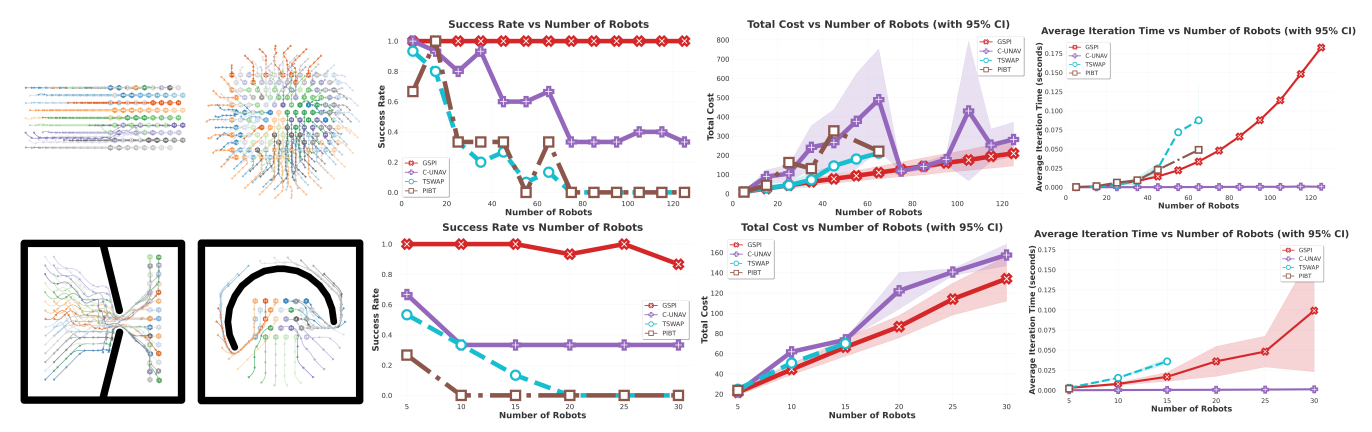


Figure 3: Extreme scalability analysis for GSPI. Across two different problem sets—empty environments with extreme robot density on the top row and obstacles-laden environments that require careful coordination on the bottom row—we tested GSPI and baselines on 270 planning problems each. Left to right: (a) Illustrations of scenarios. Note that, if robots were not allowed to swap goals, their indices would have been sorted in a row-major order. (b) Success rate results show GSPI solving significantly more problems than baselines. (c) Cost comparisons show GSPI being on-par or improving on solution costs obtained by baselines. (d) Time per iteration is short for GSPI and increases with the problem complexity.

methods, a clear hierarchy emerged. The discrete–continuous cogeneration approach (GCo_{DC}) dominated, achieving the highest success rates and lowest costs, with GCo_{CC} and GCo_{CT} trailing it but still outperforming the baseline. Because all other components of the planners were identical, this performance gap underscores the stability advantages of combining discrete contact-point selection with continuous trajectory generation.

5.3 GSPI Extreme Scalability Analysis

Finally, we evaluated GSPI, the motion-planning component of GCo, on large-scale AMRMP problems, where many robots were required to navigate to interchangeable goals in cluttered maps.

5.3.1 Evaluated Methods. We compared GSPI to state-of-the-art and adapted baselines. The primary comparator was the centralized variant of DEC-UNAV [7], referred to as C-UNAV, which uses ORCA [32] for navigation and swaps goals between robots when doing so reduces an energy function. For our experiments, we modified the official ORCA implementation released by the same authors⁴, adding the goal-swapping mechanism. One of our goal-swapping conditions in GSPI—the check for system cost—was inspired by this method. We also included TSWAP and PIBT, both naïvely adapted to use motion primitives. The motion primitives we used for TSWAP, PIBT, and GSPI were short (5 cm) motions in eight cardinal directions. Since all methods operate iteratively, committing to one motion primitive at a time, we also report iteration time, defined as the average compute time required to commit to a move.

5.3.2 **Test Problems**. We evaluated all methods on six representative maps, four of which are illustrated in Fig. 3. Each map had fixed start and goal sets and was repeated five times with random initial assignments. In the first three maps, which were obstacle-free, we scaled team sizes from five to 125, and in the latter three, which contained dense obstacles, the number of robots scaled to 30. GSPI, C-UNAV, and TSWAP leveraged goal swaps, while PIBT did not.

We include PIBT due to its algorithmic similarity to GSPI to isolate the significance of goal swapping within the PIBT structure.

5.3.3 **Results**. Our results demonstrate that GSPI is empirically effective for large-scale AMRMP. It consistently solved more problems than competing methods, with lower or comparable solution costs. PIBT fared poorly due to livelocks, and TSWAP frequently deadlocked under motion primitives. C-UNAV performed much better but still suffered from deadlocks when goals were tightly packed and, at times, robots getting stuck behind static obstacles. To the best of our understanding, this behavior was due to C-UNAV's reliance on ORCA, which excels at robot-robot avoidance but, in our experience, struggled with static obstacles even after substantial parameter tuning efforts. In contrast, GSPI maintained robustness across all tested scales, including problems with over 100 robots, highlighting its scalability in AMRMP.

6 CONCLUSION

We introduced GCo, a unified framework for collaborative multirobot, multi-object non-prehensile manipulation that combines the strengths of generative modeling and multi-robot motion planning. At its core, GCo leverages flow-matching co-generation to propose contact formations and manipulation trajectories directly from perception, and integrates them with GSPI, a new scalable algorithm for anonymous multi-robot motion planning. This combination enables robots not only to decide *how* to interact with objects, but also to coordinate efficiently across large teams and dense clutter.

Through extensive experiments, we demonstrated that GCo consistently outperformed reinforcement learning and heuristic baselines in single- and multi-object manipulation, and that the discrete-continuous instantiation delivered the best performance. Moreover, we showed that GSPI achieved substantial scalability in AMRMP, successfully solving dense problems with more than one hundred robots where prior approaches struggle. In this light, we find that generative co-design, coupled with lightweight planning, is a powerful recipe for collaborative manipulation.

 $^{^4} https://github.com/PathPlanning/ORCA-algorithm \\$

REFERENCES

- Kevin Black, Noah Brown, Danny Driess, Adnan Esmail, Michael Equi, Chelsea Finn, Niccolo Fusai, Lachy Groom, Karol Hausman, Brian Ichter, et al. 2024. π: A Vision-Language-Action Flow Model for General Robot Control. CoRR (2024).
- [2] Andrew Campbell, Jason Yim, Regina Barzilay, Tom Rainforth, and Tommi Jaakkola. 2024. Generative Flows on Discrete State-Spaces: Enabling Multimodal Flows with Applications to Protein Co-Design. In *International Conference* on Machine Learning. PMLR.
- [3] Joao Carvalho, An TLe, Mark Baierl, Dorothea Koert, and Jan Peters. 2023. Motion planning diffusion: Learning and planning of robot motions with diffusion models. In IEEE/RSJ International Conference on Intelligent Robots and Systems (IROS).
- [4] Jianing Chen, Melvin Gauci, Wei Li, Andreas Kolling, and Roderich Groß. 2015. Occlusion-based cooperative transport with a swarm of miniature mobile robots. IEEE Transactions on Robotics 31, 2 (2015), 307–321.
- [5] Cheng Chi, Zhenjia Xu, Siyuan Feng, Eric Cousineau, Yilun Du, Benjamin Burch-fiel, Russ Tedrake, and Shuran Song. 2023. Diffusion policy: Visuomotor policy learning via action diffusion. The International Journal of Robotics Research (2023).
- [6] Benjamin J. Cohen, Sachin Chitta, and Maxim Likhachev. 2010. Search-based planning for manipulation with motion primitives. In 2010 IEEE International Conference on Robotics and Automation. 2902–2908. https://doi.org/10.1109/ ROBOT.2010.5509685
- [7] Stepan Dergachev and Konstantin Yakovlev. 2024. Decentralized Unlabeled Multi-agent Navigation in Continuous Space. In International Conference on Interactive Collaborative Robotics. Springer, 186–200.
- [8] Yuming Feng, Chuye Hong, Yaru Niu, Shiqi Liu, Yuxiang Yang, and Ding Zhao. 2025. Learning Multi-Agent Loco-manipulation for Long-Horizon Quadrupedal Pushing. In IEEE International Conference on Robotics and Automation (ICRA).
- [9] Caelan Reed Garrett, Rohan Chitnis, Rachel Holladay, Beomjoon Kim, Tom Silver, Leslie Pack Kaelbling, and Tomás Lozano-Pérez. 2021. Integrated Task and Motion Planning. Annual Review of Control, Robotics, and Autonomous Systems 4, 1 (2021), 265–293. https://doi.org/10.1146/annurev-control-091420-084139 arXiv:https://doi.org/10.1146/annurev-control-091420-084139
- [10] Itai Gat, Tal Remez, Neta Shaul, Felix Kreuk, Ricky TQ Chen, Gabriel Synnaeve, Yossi Adi, and Yaron Lipman. 2024. Discrete flow matching. Advances in Neural Information Processing Systems (2024).
- [11] Valentin N. Hartmann, Andreas Orthey, Danny Driess, Ozgur S. Oguz, and Marc Toussaint. 2023. Long-Horizon Multi-Robot Rearrangement Planning for Construction Assembly. *IEEE Transactions on Robotics* 39, 1 (2023), 239–252. https://doi.org/10.1109/TRO.2022.3198020
- [12] Sigmund H Høeg, Aksel Vaaler, Chaoqi Liu, Olav Egeland, and Yilun Du. 2025. Hybrid Diffusion for Simultaneous Symbolic and Continuous Planning. Robotics: Science and Systems (RSS) (2025).
- [13] Wolfgang Hönig, Scott Kiesel, Andrew Tinka, Joseph Durham, and Nora Ayanian. 2018. Conflict-based search with optimal task assignment. In Proceedings of the International Joint Conference on Autonomous Agents and Multiagent Systems.
- [14] Wolfgang Hönig, James A Preiss, TK Satish Kumar, Gaurav S Sukhatme, and Nora Ayanian. 2018. Trajectory planning for quadrotor swarms. IEEE Transactions on Robotics (2018).
- [15] Philip Huang, Ruixuan Liu, Changliu Liu, and Jiaoyang Li. 2025. Apex-mr: Multirobot asynchronous planning and execution for cooperative assembly. *Robotics: Science and Systems (RSS)* (2025).
- [16] Jiaoyang Li, Zhe Chen, Daniel Harabor, Peter J Stuckey, and Sven Koenig. 2022. MAPF-LNS2: fast repairing for multi-agent path finding via large neighborhood search. In Proceedings of the AAAI Conference on Artificial Intelligence, Vol. 36. 10256–10265.
- [17] Jiaoyang Li, Wheeler Ruml, and Sven Koenig. 2021. Eecbs: A bounded-suboptimal search for multi-agent path finding. In Proceedings of the AAAI Conference on Artificial Intelligence, Vol. 35. 12353–12362.
- [18] Yaron Lipman, Ricky TQ Chen, Heli Ben-Hamu, Maximilian Nickel, and Matthew Le. 2022. Flow Matching for Generative Modeling. In The Eleventh International Conference on Learning Representations.
- [19] Yaron Lipman, Marton Havasi, Peter Holderrieth, Neta Shaul, Matt Le, Brian Karrer, Ricky T. Q. Chen, David Lopez-Paz, Heli Ben-Hamu, and Itai Gat. 2024. Flow Matching Guide and Code. arXiv:2412.06264 [cs.LG] https://arxiv.org/abs/ 2412.06264
- [20] Ofir Nachum, Michael Ahn, Hugo Ponte, Shixiang Gu, and Vikash Kumar. 2019. Multi-Agent Manipulation via Locomotion using Hierarchical Sim2Real.
- [21] NVIDIA. [n.d.]. Isaac Sim. https://github.com/isaac-sim/IsaacSim
- [22] Keisuke Okumura. 2023. LaCAM: Search-Based Algorithm for Quick Multi-Agent Pathfinding. In Proceedings of AAAI Conference on Artificial Intelligence (AAAI).
- [23] Keisuke Okumura and Xavier Défago. 2023. Solving Simultaneous Target Assignment and Path Planning Efficiently with Time-Independent Execution. Artificial Intelligence (2023), 103946. https://doi.org/10.1016/j.artint.2023.103946
- [24] Keisuke Okumura, Manao Machida, Xavier Défago, and Yasumasa Tamura. 2019. Priority Inheritance with Backtracking for Iterative Multi-agent Path Finding. In Proceedings of the Twenty-Eighth International Joint Conference on Artificial

- $\label{ligence} \emph{Intelligence, IJCAI-19.} \ International Joint Conferences on Artificial Intelligence Organization, 535–542. \ https://doi.org/10.24963/ijcai.2019/76$
- [25] Yorai Shaoul, Itamar Mishani, Maxim Likhachev, and Jiaoyang Li. 2024. Accelerating Search-Based Planning for Multi-Robot Manipulation by Leveraging Online-Generated Experiences. In 34th International Conference on Automated Planning and Scheduling.
- [26] Yorai Shaoul, Rishi Veerapaneni, Maxim Likhachev, and Jiaoyang Li. 2024. Unconstraining multi-robot manipulation: Enabling arbitrary constraints in ecbs with bounded sub-optimality. In Proceedings of the International Symposium on Combinatorial Search.
- [27] Guni Sharon, Roni Stern, Ariel Felner, and Nathan R Sturtevant. 2015. Conflict-based search for optimal multi-agent pathfinding. Artificial Intelligence 219 (2015), 40–66.
- [28] Yimin Tang, Sven Koenig, and Jiaoyang Li. 2024. Ita-ecbs: A bounded-suboptimal algorithm for combined target-assignment and path-finding problem. In Proceedings of the International Symposium on Combinatorial Search, Vol. 17. 134–142.
- [29] Yimin Tang, Zhongqiang Ren, Jiaoyang Li, and Katia Sycara. 2023. Solving multi-agent target assignment and path finding with a single constraint tree. In 2023 International Symposium on Multi-Robot and Multi-Agent Systems (MRS). IEEE, 8-14.
- [30] Zili Tang, Yuming Feng, and Meng Guo. 2024. Collaborative Planar Pushing of Polytopic Objects with Multiple Robots in Complex Scenes. arXiv preprint arXiv:2405.07908 (2024).
- [31] Emanuel Todorov, Tom Erez, and Yuval Tassa. 2012. Mujoco: A physics engine for model-based control. In IEEE/RSJ international conference on intelligent robots and systems.
- [32] Jur Van Den Berg, Stephen J Guy, Ming Lin, and Dinesh Manocha. 2011. Reciprocal n-body collision avoidance. In Robotics Research: The 14th International Symposium ISRR. Springer, 3–19.
- [33] Ziyan Xiong, Bo Chen, Shiyu Huang, Wei-Wei Tu, Zhaofeng He, and Yang Gao. 2024. Mqe: Unleashing the power of interaction with multi-agent quadruped environment. In 2024 IEEE/RSJ International Conference on Intelligent Robots and Systems (IROS).
- [34] Jingjin Yu and Steven M LaValle. 2013. Multi-agent path planning and network flow. In Algorithmic Foundations of Robotics X: Proceedings of the Tenth Workshop on the Algorithmic Foundations of Robotics.



Figure 4: MuJoCo environments for our single-object experiments. Left: *Empty* with three robots, going up. Middle: *Easy* with two robots, going right. Right: *Slalom* with one robot, going up.

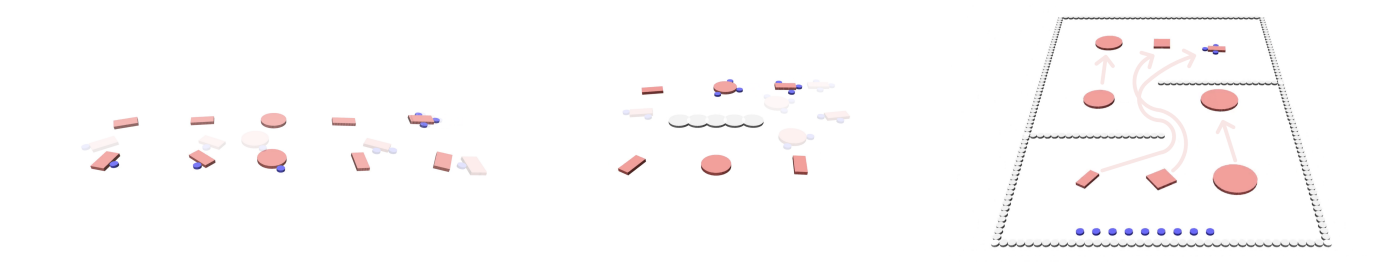


Figure 5: MuJoCo environments for our multi-object experiments. Left: *Empty* with three robots and five objects, going up. Middle: *Wall* with six robots, going up. Right: *Slalom* with nine robots, going up, marked with arrows to avoid clutter.

A ADDITIONAL EXPERIMENTAL DETAILS

In this appendix section, we will provide more details and illustrations for our experiments and implementations.

A.1 Manipulation Experiments

As discussed in Sec. 5.1 and Sec. 5.2, we conducted our manipulation experiments in two main settings: single-object and multi-object manipulation. For both, we modeled robots as cylinders in MuJoCo (shown in blue in Fig. 4 and Fig. 5), and modeled movable objects as extruded circular and polygonal shapes (shown in red in the same figures). We used Isaac-Sim [21] to visualize our experiments (Fig. 1, Fig. 2).

We include additional results for the cost metric in our manipulation experiments. As shown in Fig. 6, we observed that the GCo methods consistently utilized their available resources effectively, decreasing the average distance per robot as the number of available robots increased. In practice, this translates to more effective manipulation with more robots per object, and to less fluctuation between contact points. As previously noted, our current allocation scheme is simple and has room for further research. We leave this to future work.

B GSPI THEORETICAL ANALYSIS

In our manuscript, we outlined the GSPI algorithm and discussed its practical performance. Here, we provide intuition for GSPI's strong empirical results and sketch a completeness proof under similar

assumptions made by Dergachev and Yakovlev [7] in their analysis of C-UNAV⁵. Let us begin with a formal definition of *completeness*:

Definition B.1 (Completeness in AMRMP). An AMRMP algorithm is complete if, whenever collision-free trajectories exist that bring all robots from their starts to distinct goals and allow them to remain there indefinitely, it is guaranteed to find such trajectories.

For proving the completeness of C-UNAV [7], the authors assumed access to a "complete non-anonymous motion planner" that, given a goal assignment for all robots, can convey those to their goals in a safe manner. In practice, Dergachev and Yakovlev [7] implemented their algorithm with ORCA as their non-anonymous motion planning algorithm and noted that it can deadlock (i.e., it is not complete). We follow a similar reasoning here. We will first assume that we have access to a non-anonymous motion planner, show that under that assumption GSPI is complete, and then outline a potential approach to proving a stronger notion of completeness for GSPI that does not rely on such an assumption. Although we do not provide such a proof here, we have found no counterexamples to date, which makes us optimistic about GSPI's overall completeness.

⁵We would like to acknowledge the similarity between GSPI and the work by [7], and thank the authors for their contributions. The GSPI goal swapping condition can be seen as an extension of C-UNAV, in that it not only reasons over a swap's benefit to the system, but also considers the priority of robots. In practice, GSPI does not exhibit deadlocks while C-UNAV, which leverages ORCA for collision avoidance, may occasionally deadlock or fail to avoid static obstacles.

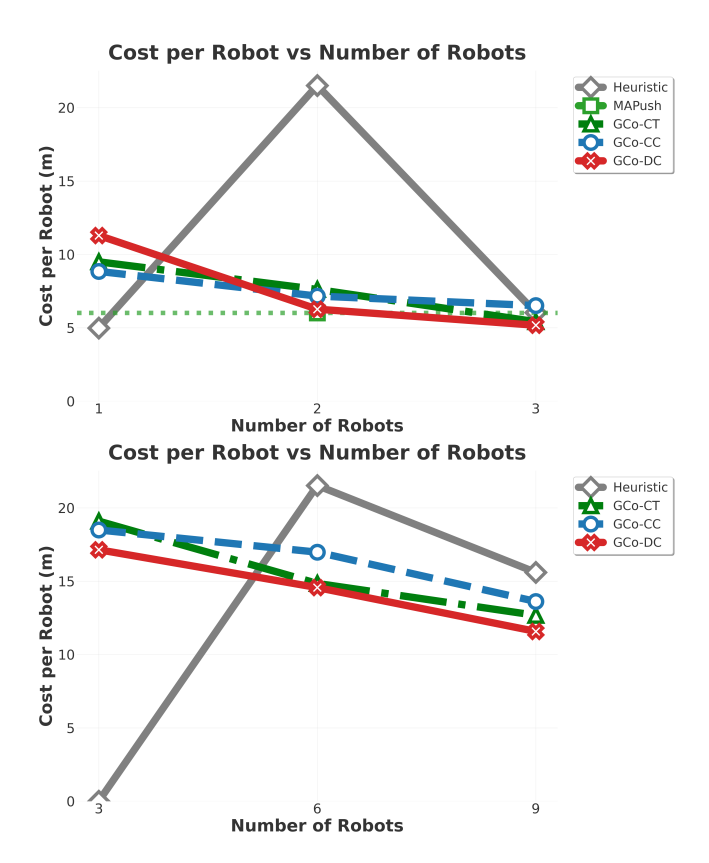


Figure 6: Additional results from our manipulation experiments showing the average cost per robot breakdown. We observe that GCo methods have a reduced cost per robot as the nuber of available robots in the environments increases. This sheds light on GCo's ability to effectively utilize the resources at its disposal.

Assumption 1. For an injective mapping between robots and goals, PIBT for circular planar robots moving with identical motion primitives ensures that each robot eventually reaches its assigned goal. However, remaining at the goal indefinitely is not guaranteed.

In other words, the highest-priority robot in PIBT makes monotone progress toward its assigned goal, possibly at the expense of temporarily displacing robots already at their goals. This parallels PIBT's guarantees in the discrete MAPF setting. Under this assumption, we now show that GSPI is complete.

LEMMA B.2 (MONOTONE PROGRESS). GSPI ensures that the highest-priority robot makes monotone progress toward its (possibly changing) assigned goal.

PROOF. The highest-priority robot in GSPI executes two procedures: TRYSWAP and TRYMOVE.

Swap. By definition, a goal swap is permitted only if it *strictly reduces* the high-priority robot's distance to a goal, while not increasing the overall system cost. Thus, goal swaps in GSPI are permissible.

Move. By Assumption 1, PIBT guarantees that the highest-priority robot can eventually reach its assigned goal under motion primitives. In GSPI, TRYMOVE inherits this property: either the robot moves directly, or priority inheritance recursively propagates displacement requests until the blockage is resolved, ensuring eventual progress.

Therefore, in both cases, the highest-priority robot's distance to a goal strictly decreases over time. This proves monotone progress.

LEMMA B.3 (STABILITY AT GOALS). GSPI ensures that robots can eventually remain at their goals indefinitely.

PROOF. PIBT fails to guarantee stability at goals because of *priority fluctuation*: when a robot arrives at a goal, its priority drops, allowing higher-priority robots to displace it repeatedly, creating livelocks.

GSPI resolves this issue with *goal swapping*. Suppose a high-priority robot displaces a lower-priority robot already at its goal. By construction, the high-priority robot's original goal must be farther away than the one it is displacing toward. The swap condition ensures that exchanging goals strictly decreases the overall system cost. Consequently, the high-priority robot adopts the nearer goal, while the displaced robot receives the farther one.

Since each swap reduces the total system cost, swaps cannot continue indefinitely. Eventually, all robots will stabilize into assignments where no further swaps are beneficial, and each robot can remain at its goal indefinitely.

Even in degenerate cases where physical motion is impossible (e.g., a tightly-packed configuration), goal assignments will still converge to a stable state through the swap mechanism alone.

Theorem B.4 (Completeness under Assumption). Under Assumption 1, GSPI is complete: if there exist trajectories conveying robots to goals (in any valid assignment permutation), GSPI will find one set of such trajectories.

PROOF. From Lemma B.2, the highest-priority robot always makes progress toward a goal. From Lemma B.3, at some point in time, robots can remain at goals. Thus, all robots reach distinct goals and remain there indefinitely. This establishes completeness under Assumption 1.

B.1 Toward a Stronger Proof

The main remaining gap is Assumption 1. To prove completeness without it, one must show that PIBT with motion primitives can guarantee progress for the highest-priority robot. That is, given fixed goals, it must guarantee delivery of all robots to their goals without deadlock (but potentially with livelock).

We outline a potential roadmap toward such a proof. The main difference between PIBT on robots with a footprint that move along motion primitives and the simplified MAPF case is that, in the new setting, a robot considering a candidate motion primitive may find itself colliding with more than one other robot. In the original MAPF case, a robot could only "step on" a single other robot. There, ensuring that the highest-priority robot could always move effectively (i.e., reduce its distance to goal) boiled down to showing that the underlying MAPF graph is bi-connected. That is, the highest-priority

55

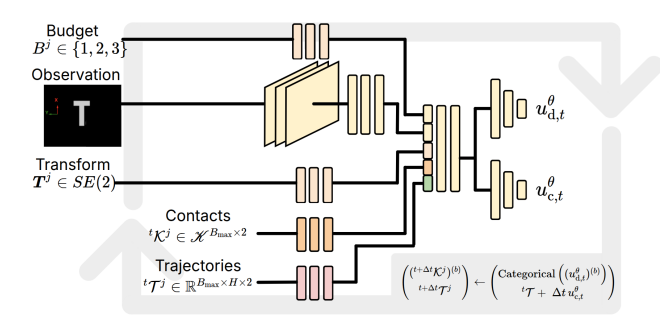


Figure 7: GCo co-generation model diagram. Given inputs of a robot budget, an object observation, and a requested transformation, GCo_{DC} jointly produces contact points and manipulation trajectories for moving the object as requested.

robot could push a cycle of robots along a loop that includes its current vertex and goal vertex and move toward its goal. In other words, the recursive calls induced by priority inheritance are a *chain* – a single recursive branch. In the motion primitives case, a situation where a robot's tentative motion primitive overlaps with multiple other robots yields multiple recursive chains, and has each recursive call treat the previous calls as higher priority. Say the first recursive call includes the robots $\{R^1, R^2, R^3\}$ and the second recursive call includes $\{R^4, R^5, R^6\}$. Currently, GSPI sets

$$\{R^1, R^2, R^3\} \prec \{R^4, R^5, R^6\}$$

and tries all orderings of recursive chains. GSPI, however, never explores cross-chain priorities, for example,

$$(R^1 \prec R^4) \land (R^5 \prec R^2).$$

What remains to be shown for completeness (or counter, for lack of) is that this exhaustive exploration of all priority combinations

between robots is unnecessary for allowing Gspi's highest-priority robot to make progress. Doing so would eliminate reliance on Assumption 1 and establish a stronger completeness guarantee for Gspi in continuous multi-robot motion planning.

B.2 A Note on "Completeness" vs. Efficiency

We have observed that removing the enumeration of all orderings of TRYMOVE recursive calls within the set *S* of "stepped-on" robots can, at times, dramatically improve runtimes. We have scaled experimentation to over 200 robots with this small change and would recommend it to practitioners.

C IMPLEMENTATION DETAILS

 $C.0.1\,$ Neural Networks. All neural networks were implemented in Python with PyTorch, and our AMRMP algorithm, GSPI, was implemented in C++ and exposed via Python bindings. Our flow-matching implementations build on the code from Lipman et al. [19]. We would like to acknowledge their excellent work on making flow-matching theory and practice available and clearly communicated. Importantly, GCo only requires training a single network for all object types and sizes, as well as for handling variable budgets $B_{\rm max}$. An illustration of our co-generation network in Fig. 7.

C.0.2 Robot Budget. We used $B_{\text{max}} = 3$ in all of our models, with training data including examples with 1, 2, and 3 robots per object.

C.0.3 Code Availability. Our code will be made available online at gco-paper.github.io.

C.0.4 Experiment and Training Setup. All training and experiments were done on a laptop with an Nvidia RTX 3080-Ti GPU and an Intel Core i9-12900H with 32GB RAM (5.2GHz).